Supplemental Data

Supplemental Methods

Genotyping. To genotype the H-*Ras*^{LSLG12V} and H-*Ras*^{G12V} alleles, we submitted tail DNA to PCR analysis at 94 ºC for 1 min, followed by 35 cycles of 94 ºC denaturing for 30 s, 60 ºC annealing for 30 s, and 72 ºC extension for 1 min, followed by an elongation cycle of 72 ºC for 10 min with the following primers: 5' forward wild-type primer (H-*Ras*F-B1, 5'-TCTAATTTGGGTGCGTGGTTG-3'), forward STOP primer (stopF-B3, 5'-TCAGCCATACCACATTTGTAGAGG-3'), and reverse primer (H-*Ras*R-B2, 5'-CCACTTGAGACGGCTAATAGATGC-3'). The sizes of the diagnostic PCR products are 230 bp (B1:B2) and 490 bp (B2:B3) for the wild-type and for the targeted H-*Ras*^{LSLG12V} allele, respectively. In tissues in which the floxed STOP cassette present in the targeted H-*Ras* allele has been excised (H-*Ras*^{G12V}), primers B1:B2 yield a DNA fragment of 430 bp. For H-*Ras*^{geo} allele we perform same PCR protocol with the following primers: 5' forward primer (H-*RasEx4*F-13B1, 5'-TGCAGTCAGTCATGTCCTTTGTGC-3'), reverse H-*Ras*^{geo} primer (NeoF-2B1, 5'-TGACCGCTTCCTCGTGCTT-3'), and reverse wild type primer (H-*RasEx4*R, 5'-AGTGGCAACAGGGACAGTTCAT-3'). The sizes of the diagnostic PCR products are 210 bp and 320 bp for the wild-type and for the targeted H-*Ras*^{geo} allele, respectively.

Histopathology and immunohistochemistry. Embryos and tissues including adipose tissue (brown and white), adrenal gland, bone marrow, brain, eye, Harderian gland, heart and aorta, intestine (small and large), kidney, liver, lung, mammary gland, ovary, pancreas, pituitary, prostate, skeletal muscle, salivary gland, skin, spleen, stomach, thymus, testis, thyroid, urinary bladder and uterus were dissected, fixed in 10%-buffered formalin (Sigma) and embedded in paraffin. Three- or five-micrometer-thick sections

were stained with hematoxylin and eosin (H&E). Antibodies used for immunohistochemistry analysis included mouse monoclonal anti-cytokeratin 8 (Troma I) (1:25 dilution, Hibridoma Bank); rabbit polyclonal anti-cytokeratin 14 (1:25 dilution, Neomarkers); mouse monoclonal anti-pankeratin AE1-AE3 (1:25 dilution, Neomarkers); rabbit polyclonal anti-estrogen receptor α (1:150 dilution, Santa Cruz); rabbit monoclonal anti-progesterone receptor (prediluted, LabVision), rabbit polyclonal to phospho-Erk (1:25 dilution, Cell Signalling) and rabbit polyclonal to TGFβ1(1:75 dilution, Santa Cruz). Identification of elastic fibers in lip skin was performed by orcein staining of paraffin sections. Chondroitin-bearing proteoglycans detection was performed by Alcian blue staining of several paraffin-embeded tissues at pH 2.5. For whole mount studies of mammary glands, tissue was placed on dry, silanized glass slides and fixed overnight in Carnoy's fixative (1:3:6 parts of glacial acetic acid, chloroform and 100% ethanol, respectively). Tissues were rehydrated through successive incubations with 70% ethanol followed by distilled water, and stained with Red Carmine overnight. For detection of β-galactosidase activity in embryos and adult tissues, samples were included in O.C.T.^{TM} compound (Sakura) and frozen. X-Gal staining of 10 μm thick cryosections was performed as described (1). Counter-staining of cryostat sections was performed with nuclear fast red.

Electron microscopy analyses. Hearts were collected from one month–old mice perfused with 0.1 M phosphate buffer (pH 7.4) containing 4% paraformaldehyde and 1% glutaraldehyde, cut using an Ultracut E apparatus (Reichert-Jung), post-fixed in 1% OsO_4 in 0.1 M phosphate buffer (pH 7.4), dehydrated with acetone and embedded in Araldite-Durcupan resin (Sigma). Semi-thin sections were used to localize and orient the tissues. Subsequently, ultra-thin sections were cut and stained with uranyl acetate

(Emscope) and lead citrate (Merck) for electron microscopy analysis.

Electrocardiogram analysis. Electrocardiographic recordings on four month–old animals were obtained using a Data Sciences International telemetry system (Saint Paul, MN). To this end, radiofrequency transmitters were placed in the abdominal cavity of the mice, the positive lead near the left forelimb, and the negative lead near the right forelimb. Mice were placed in individual cages for data acquisition. One week after the implantation of the transmitter, electrocardiographic data were collected and analyzed with the Dataquest A.R.T v4.0 acquisition and analysis software (Data Sciences International).

AngII signaling pathway. Levels of *Agt*, *Ren, Ace, Agtr1a, Agtr2, Ednra* and *Ednrb* mRNAs were determined by quantitative, real-time reverse–transcription PCR as previously described (2). The sequences of primers used are available upon request. ACE activity in heart extracts was determined using a luminescence method as previously described (2). For the blood vessel reactivity study, renal arteries were cannulated and perfused at 1 ml/min with a Krebs-Henseleit solution (118.4 mM NaCl, 4.7 mM KCl, 2 mM $CaCl_2$, 1.2 mM $MgSO_4$, 1.2 mM KH_2PO_4, 25 mM $NaHCO_3$ and 11 mM glucose) at 37 °C and equilibrated with an atmosphere of 95% O_2 plus 5% CO_2. Catheters were connected to a pressure probe linked to a digital data recorder (MacLab/4e, AD Instruments). Arteries were perfused with 0.1 μM AngII (Sigma). Recordings were analyzed using the Chart v3.4 software (AD Instruments).

Supplemental References

1. Hogan, B., Beddington, R., Costantini, F., and Lacy, E. 1994. *Manipulating the Mouse Embryo: A Laboratory Manual.* Cold Spring Harbor, NY.

2. Sauzeau, V., Sevilla, M.A., Rivas-Elena, J.V., de Alava, E., Montero, M.J., Lopez-Novoa, J.M., and Bustelo, X.R. 2006. Vav3 proto-oncogene deficiency leads to sympathetic hyperactivity and cardiovascular dysfunction. *Nat. Med.* **12**:841-845.

Supplemental Figure Legends

Supplemental Figure 1. Gene targeting strategy. (**A**) Homologous recombination at the 3' region of the H-*Ras* locus. Exons (0-4) are indicated by boxes. Filled boxes, coding sequences. Open boxes, noncoding sequences. Gray box, polyadenylation sequences. Stapled box, PGK-thymidine kinase (TK) cassette. Dotted box, IRES-*β-geo* cassette. The location of the external probe (A) used in Southern blot analysis is indicated. Representative restriction enzyme sites are indicated (H, HindIII; N, NotI; Nc, NcoI; S, SpeI; X, XbaI). (**B**) Southern blot analysis of DNA isolated from wild-type H-*Ras*$^{+/+}$ and recombinant H-*Ras*$^{+/geo}$ ES clones. Migration of the corresponding alleles after digestion with XbaI is indicated by arrowheads. (**C**) Homologous recombination at the 5' region of the H-*Ras* locus. Asterisk, G12V oncogenic mutation. Checkered box, PGK-Hygromycin (Hyg) resistance cassette. Octogonal box (STOP), transcriptional inhibitory sequences. Filled triangles, loxP sites. The position of the external probe (B) used in the Southern blot analysis is indicated. (**D**) Southern blot analysis of DNA isolated from recombinant ES cell clones carrying the 3' (H-*Ras*$^{+/geo}$) and the 3' and 5' (H-*Ras*$^{+/LSLG12V}$) homologous recombination events. Migration of the corresponding alleles after digestion with SpeI is indicated by arrowheads. Identification of ES clones carrying the 5' and 3' homologous recombination events in the same H-*Ras* allele was determined by negative X-Gal staining of ES cells and confirmed by the induction of β-galactosidase activity after infection with a retrovirus carrying a bacterial Cre recombinase (data not shown). (**E**) H-*Ras*^{G12V} allele resulting from crossing H-*Ras*$^{+/LSLG12V}$ mice to *EIIaCre* transgenic animals to excise the LSL cassette.

Supplemental Figure 2. Analysis of H-*Ras* expression in E14.5 embryos. (**A-E**) Cryostat sections were submitted to X-Gal staining to determine β-galactosidase activity

as a surrogate marker for expression of H-*Ras*^{geo} alleles. (**A**) Sagital section of E14.5 embryos. Heart (arrow), dorsal root ganglia (solid arrowhead), medulla oblongata (asterisk) and spinal cord (open arrowhead) are indicated. Scale bar, 1 mm. (**B**) heart, (**C**) kidney including the adrenal gland (ad), (**D**) lung (lu) and liver (liv), (**E**) pancreas. Scale bar B-E, 20 μm.

Supplemental Figure 3. Analysis of H-*Ras* expression in adult tissues. Cryostat sections were submitted to X-Gal staining to determine β-galactosidase activity as a surrogate marker for expression of H-*Ras*^{geo} alleles. Positive staining in (**A**) heart including the endothelium (arrowheads) and in (**B**) aorta. Negative staining in (**C**) skeletal muscle. Scale bars, 10 μm.

Supplemental Figure 4. Analysis of H-*Ras* expression in additional adult tissues. Cryostat sections were submitted to X-Gal staining to determine β-galactosidase activity as a surrogate marker for expression of H-*Ras*^{geo} alleles. (**A**) Kidney section showing glomeruli (dotted line) and tubules (asterisk), (**B**) mammary gland section showing myoepithelial ductal cells (arrowhead), (**C**) skin section showing hair follicle (asterisk) and sebaceous gland (arrowhead), (**D**) urinary bladder section showing robust staining in the epithelial mucosa (asterisk), (**E**) pancreas section showing X-Gal staining in islets (i), but not in ducts (arrowhead) or acini (asterisk), (**F**) colon section showing rather uniform staining, (**G**) hippocampus and (**H**) cerebral cortex sections. Scale bars, 10 μm, except for **C,G,H**, 20μm.

Supplemental Figure 5. Analysis of H-*Ras* expression in adult lung. Cryostat sections were submitted to X-Gal staining to determine β-galactosidase activity as a surrogate

marker for expression of H-*Ras*^{geo} alleles. (**A**) Lung section illustrating robust staining in bronchiolar Clara cells (asterisk). Some type II pneumocytes also show X-Gal staining (arrowheads). (**B**) Co-staining with CC10 antibodies unequivocally identifies H-*Ras* expression in Clara cells. (**C**) Co-staining with SPC marker illustrates that only some type II pneumocytes (arrowheads) are positive for X-Gal staining. Scale bars, 10 μm.

Supplemental Figure 6. Tumor development in H-*Ras*^{G12V} mutant mice. Characterization of a mammary adenocarcinoma isolated from a one year-old H-*Ras*$^{+/G12V}$ virgin female. (**Left**) H&E staining, (**center**) Cytokeratin 8 immunostaining, (**right**) phospho-Erk immunostaining. Scale bar, 20 μm.

Supplemental Figure 7. Skin carcinogenesis in H-*Ras*^{G12V} mice. Exposure of (**top**) H-*Ras*$^{+/+}$ (n = 12), (**middle**) H-*Ras*$^{+/G12V}$ (n = 11) and (**bottom**) H-*Ras*$^{G12V/G12V}$ (n = 9) mice to DMBA+TPA treatment induced skin papillomas with similar incidence and latency. Papillomas were counted and measured once a week. Papillomas are represented according to size by open boxes (0-2 mm), dotted boxes (2-4 mm), stapled boxes (4-6 mm), light gray boxes (6-8 mm), dark gray boxes (8-10 mm) and filled boxes (>10 mm).

Supplemental Figure 8. Two dimensional analysis of sagital projections obtained by Computed Tomography of neonatal H-*Ras*$^{+/+}$ and H-*Ras*$^{G12V/G12V}$ littermates. (**Left**) Anatomic position of landmarks in a sagital section of a neonatal H-*Ras*$^{+/+}$ mouse. (**Right**). Hotteling´s T^2 test analysis of the landmarks with x and y axis of procruster

indicating significant differences in the rostral area (n = 15). (*) P < 0.01. NS, not significant.

Supplemental Figure 9. Lips of H-*Ras*^{G12V} mutant mice are engrossed. View from below of lips of representative (**Top**) H-*Ras*$^{+/+}$ and H-*Ras*$^{G12V/G12V}$ mice. Arrowhead points to the engrossed lips. (**Middle**) H&E staining. Lips of H-*Ras*$^{G12V/G12V}$ mice accumulate more adipocytes between the fascicles of muscle (asterisk), have more distended vibrissal follicles (solid arrowhead) and contain more sebaceous glands (open arrowhead). Scale bar, 50 µm. (**Bottom**) Orcein staining of lip skin reveals the presence of less and shorter elastic fibers (arrows). Scale bar, 10 µm.

Supplemental Figure 10. Ultrastructure of H-*Ras*^{G12V} cardiomyocytes. Electron microscopy was used to analyze the sarcomere organization of one month-old H-*Ras*$^{+/+}$ (n = 3) and H-*Ras*$^{G12V/G12V}$ (n = 3) mice. (**A**) Longitudinal and (**B**) transversal sections analyzed at two magnification levels. No significant differences were observed.

Supplemental Figure 11. H-*Ras* expression in aortic and pulmonary valves. (**A,B**) H&E staining of heart sections showing the aortic valve (arrowheads) of (**A**) H-*Ras*$^{geo/geo}$ and (**B**) H-*Ras*$^{G12V/G12V}$ mice. (**C,D**) Cryostat sections submitted to X-Gal staining to determine β-galactosidase activity as a surrogate marker for expression of (**C**) H-*Ras*^{geo} and (**D**) H-*Ras*^{G12V} alleles in the aortic valves. (**E,F**) H&E staining of heart sections showing the pulmonary valves (arrowheads) of (**E**) H-*Ras*$^{geo/geo}$ and (**F**) H-*Ras*$^{G12V/G12V}$ mice. (**G,H**) Cryostat sections submitted to X-Gal staining to determine β-galactosidase activity as a surrogate marker for expression of (**G**) H-*Ras*^{geo} and (**H**) H-

Ras^{G12V} alleles in the pulmonary valves. Scale bars in **A,B,E,F**, 100 μm. Scale bars in **C,D,G,H**, 20 μm.

Supplemental Figure 12. Lack of heart arrythmias in H-*Ras*^{G12V} mice. Histogram of the distribution of R-R intervals in four month–old H-*Ras*$^{+/+}$ (n = 4) and H-*Ras*$^{G12V/G12V}$ (n = 4) mice.

Supplemental Figure 13. TGFβ immunostaining. Kidney sections from four month-old (**A**) H-*Ras*$^{+/+}$ and (**B**) H-*Ras*$^{G12V/G12V}$ mice. Positive TGFβ immunostaining can be observed in areas with fibrosis in H-*Ras*$^{G12V/G12V}$ mice. Scale bar, 20 μm.

Supplemental Figure 14. The status of the rennin-AngII system in H-*Ras*^{G12V} mice. (**A**) Variation in perfusion pressures induced by renal arteries obtained from H-*Ras*$^{+/+}$ (n = 5) and H-*Ras*$^{G12V/G12V}$ (n = 6) mice upon a single administration of AngII (100 nM). **(B)** Expression levels of angiotensinogen (*Agt*), renin (*Ren*) and AngII converting enzyme (*Ace*) mRNAs in liver, kidney and hearts of four month-old H-*Ras*$^{G12V/G12V}$ mice, respectively (n = 5). The expression levels of the corresponding transcripts in H-*Ras*$^{+/+}$ mice were given an arbitrary value of 1. (**C**) Relative expression levels of the mRNAs for AngII receptor type 1 (*Agtr1a*) and AngII receptor type 2 (*Agtr2*) in aorta (closed bars), Heart (grey bars) and pulmonary artery (open bars) from four month-old H-*Ras*$^{G12V/G12V}$ mice (n = 5). The expression levels of the corresponding transcripts in H-*Ras*$^{+/+}$ mice were given an arbitrary value of 1. (**D**) Levels of ACE activity in hearts from H-*Ras*$^{+/+}$ (n = 5) and H-*Ras*$^{G12V/G12V}$ (n = 5) mice.

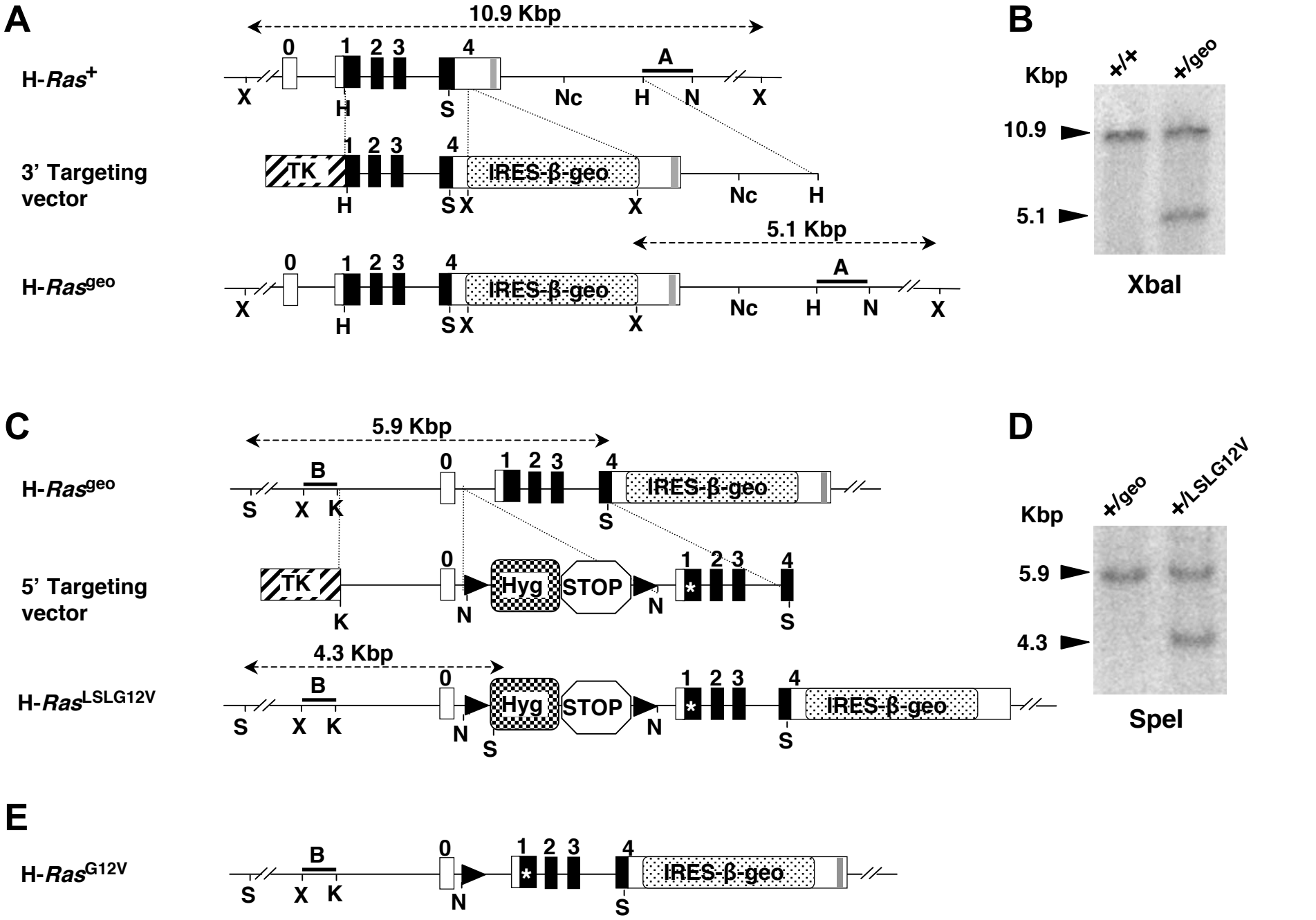
A
10.9 Kbp
H-Ras+
3' Targeting vector
H-Rasgeo
5.1 Kbp
TK
IRES-β-geo
B
Kbp
+/+
+/geo
10.9
5.1
XbaI
C
5.9 Kbp
H-Rasgeo
5' Targeting vector
4.3 Kbp
H-RasLSLG12V
Hyg
STOP
D
+/LSLG12V
5.9
4.3
SpeI
E
H-RasG12V

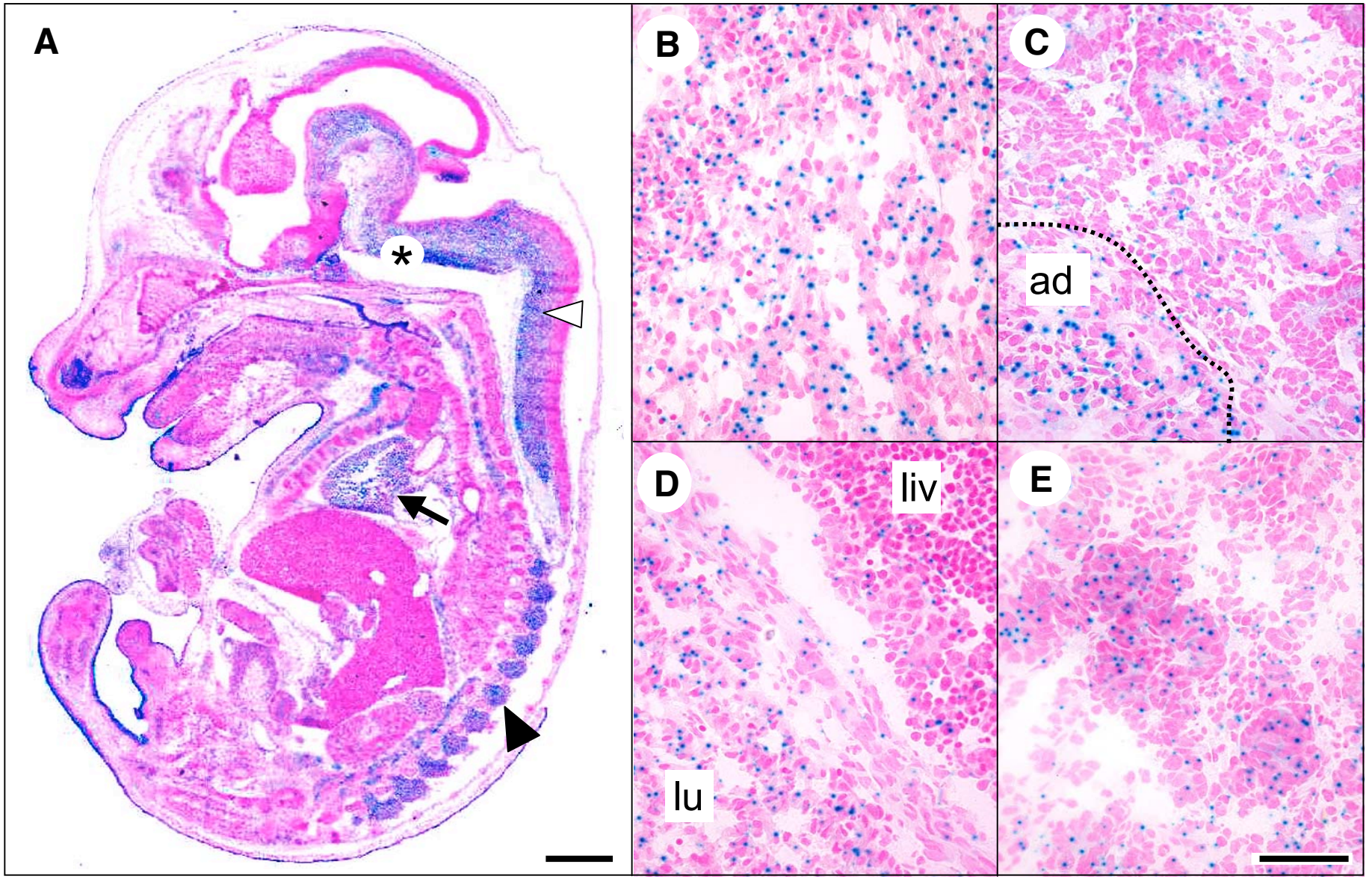
A
B
C
D
E
*
ad
liv
lu

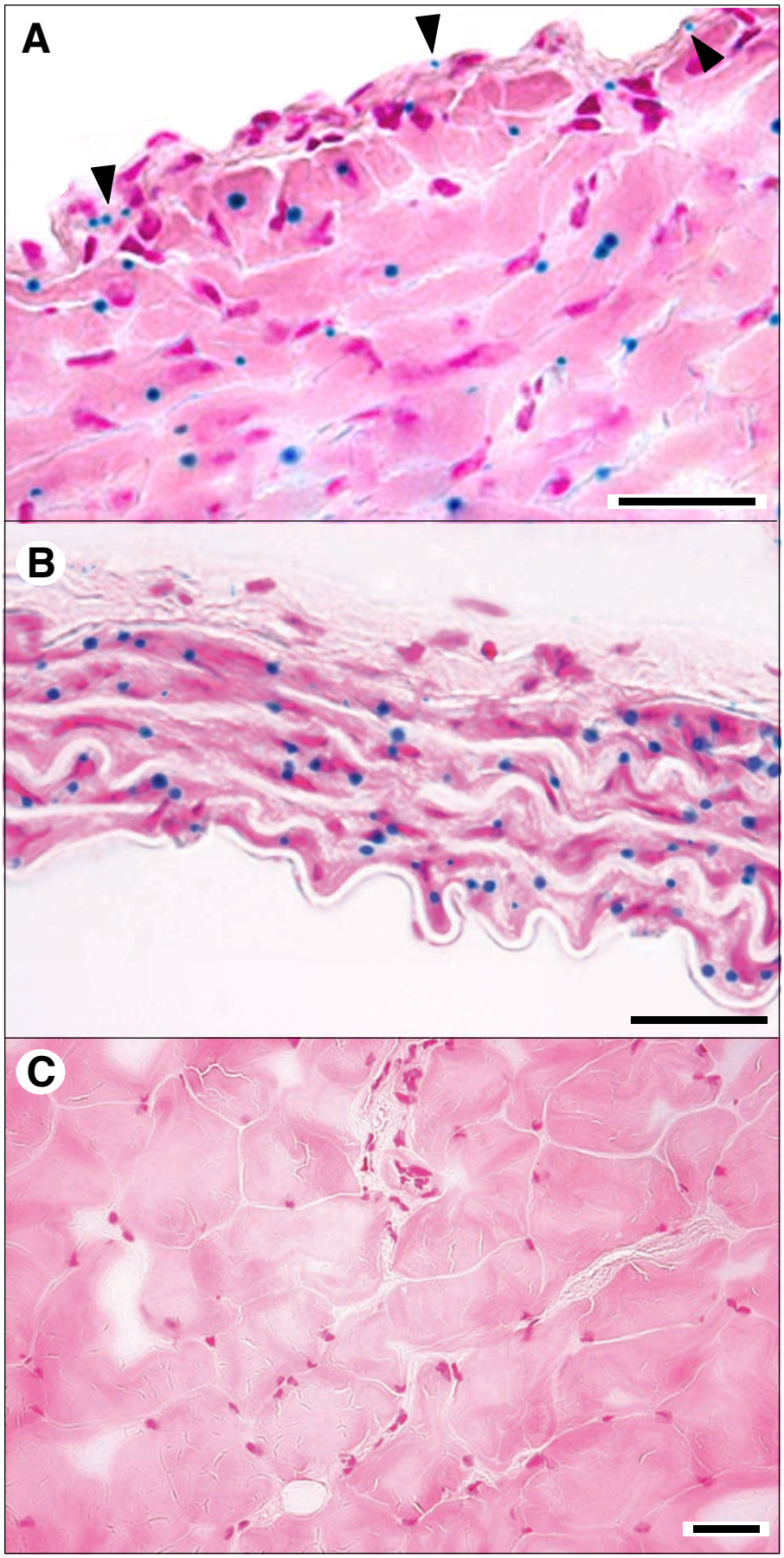
A
B
C

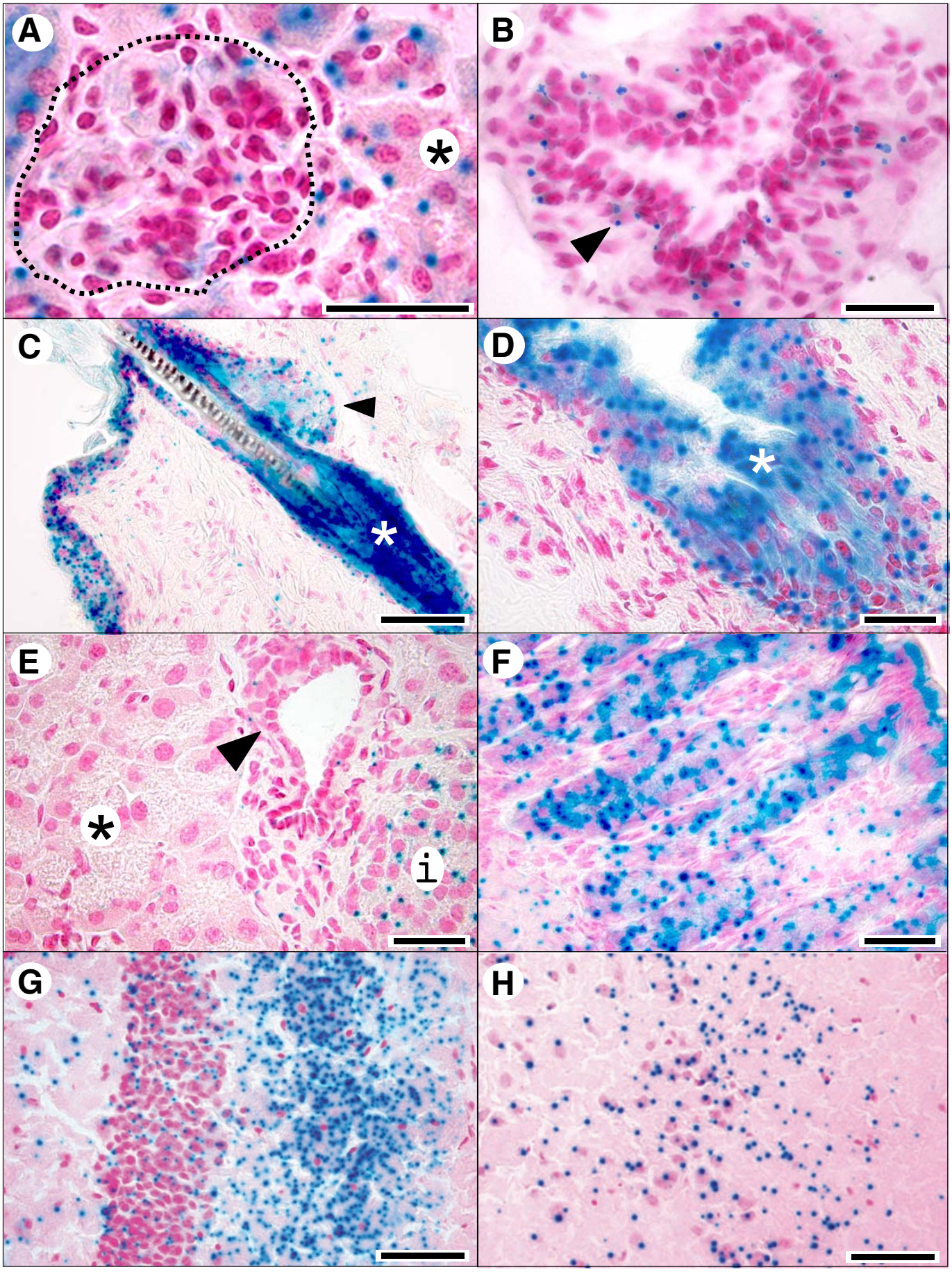
A
B
C
D
E
F
G
H
i

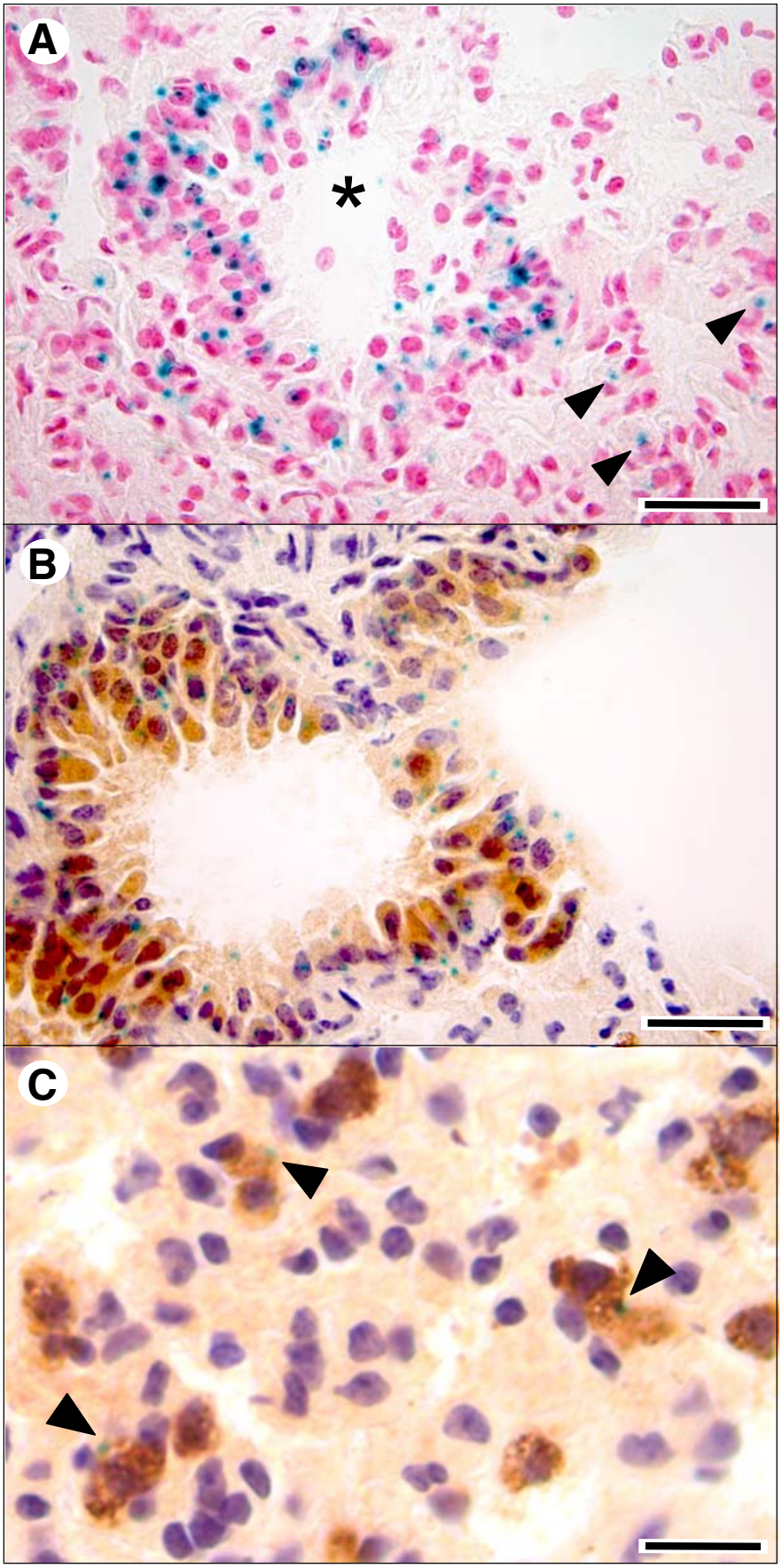
A
B
C

Mammary adenocarcinoma

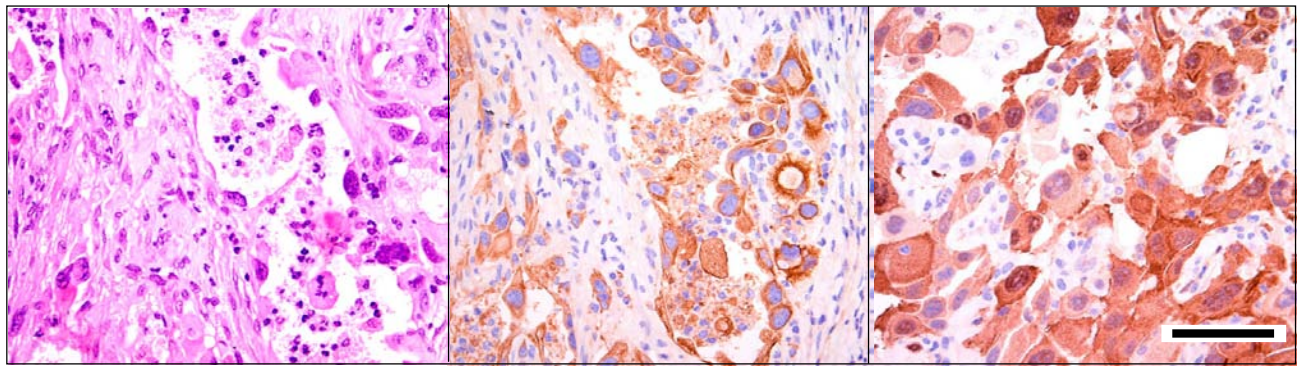

H&E staining **Cytokeratin 8** **phospho-Erk**

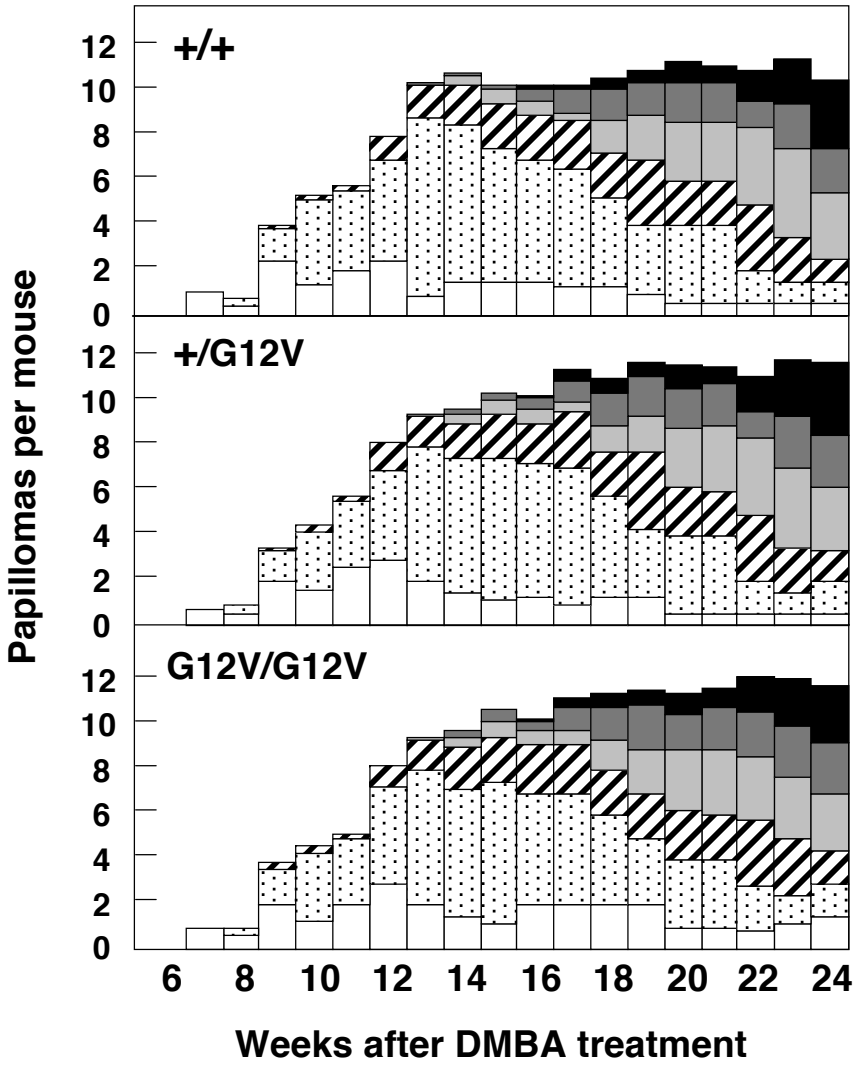
+/+
+/G12V
G12V/G12V
Papillomas per mouse
0
2
4
6
8
10
12
6
8
10
12
14
16
18
20
22
24
Weeks after DMBA treatment

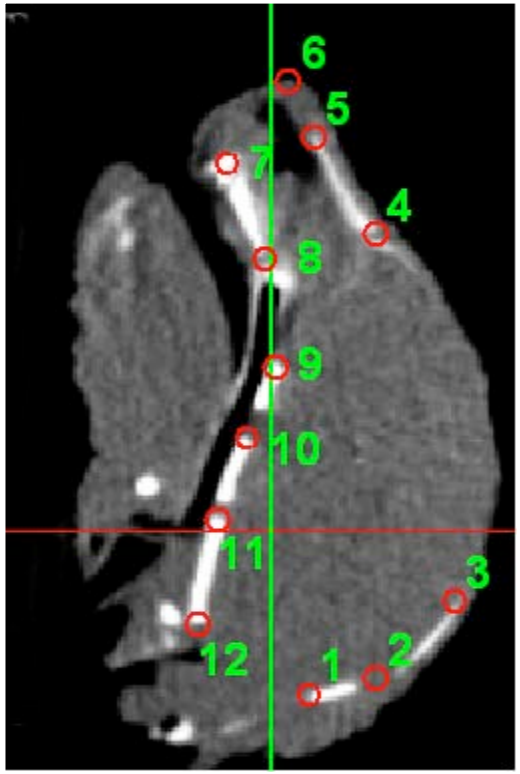

Landmarks	Anatomic position	*P* value
1	Opisthilion	NS
2	Intersection of interparietal and occipital bones	NS
3	Intersection of parietal and interparietal bones	NS
4	Nasal	0.0023*
5	Nasion	NS
6	Anterior nasal area	0.0004*
7	Center of alveolar ridge over maxillary incisor	0.0001*
8	Maxilla suture	0.0026*
9	Spheno-ethmoid synchondrosis	NS
10	Spheno-occipital synchondrosis	NS
11	Intersphenoidal suture	NS
12	Basion	NS

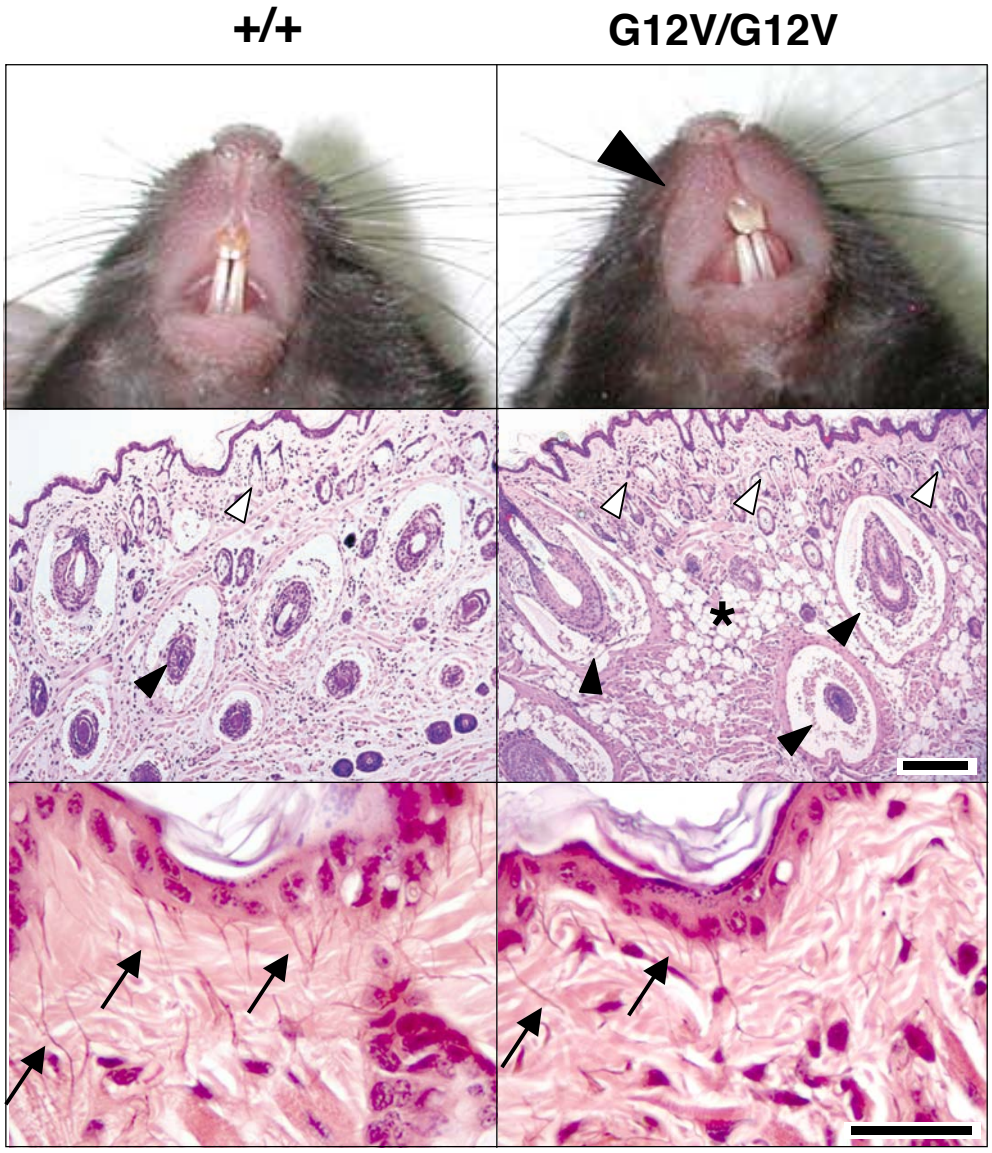
+/+
G12V/G12V

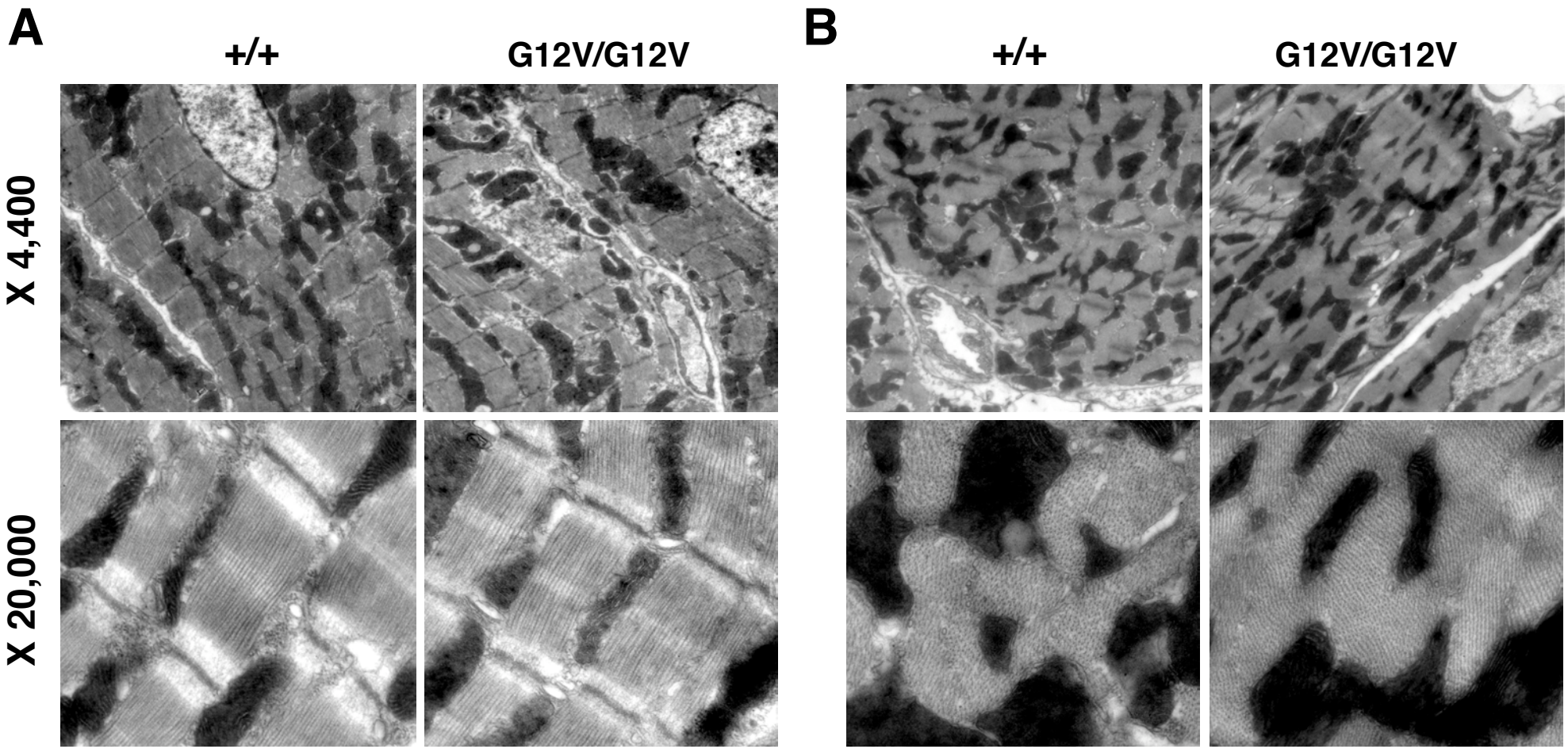
A
+/+
G12V/G12V
X 4,400
X 20,000
B
+/+
G12V/G12V

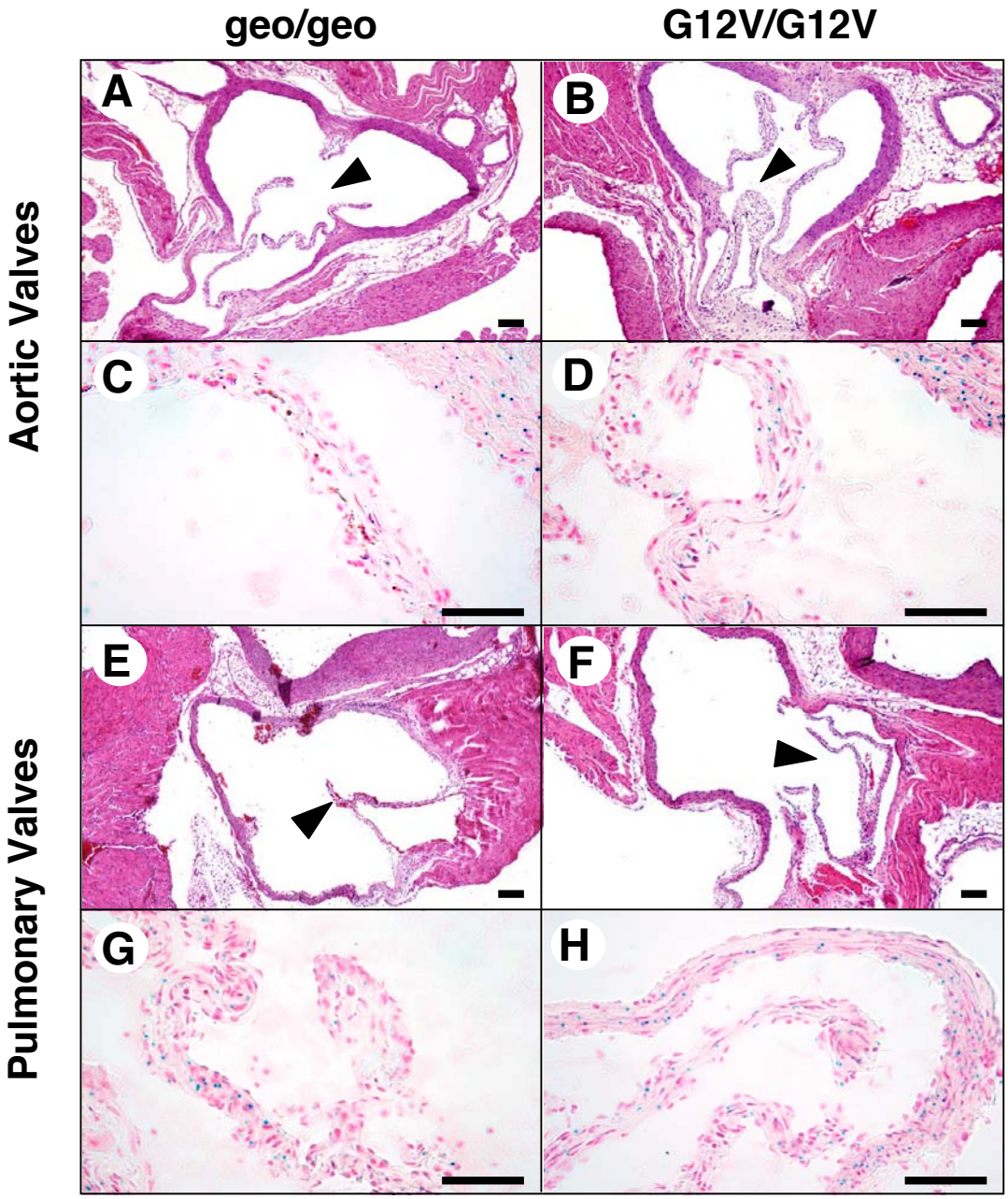
geo/geo
G12V/G12V
Aortic Valves
Pulmonary Valves
A
B
C
D
E
F
G
H

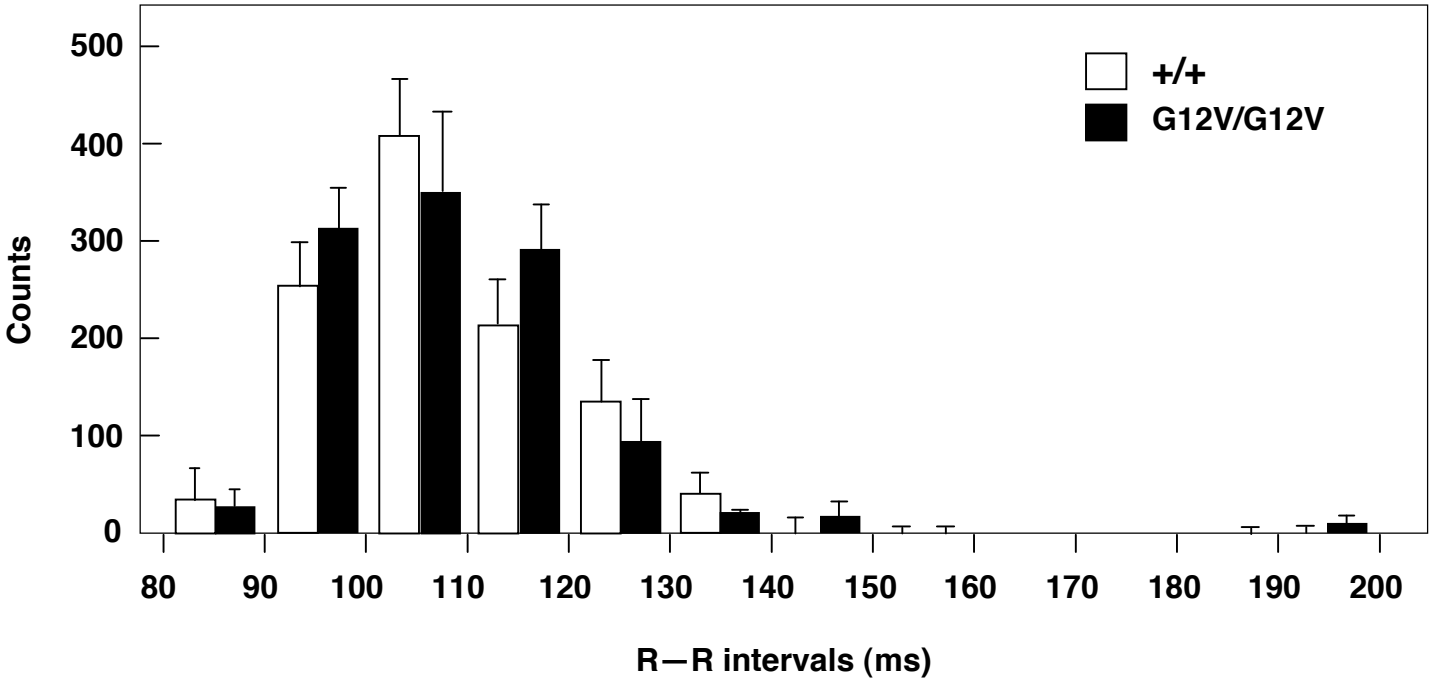
500
400
300
200
100
0
Counts
+/+
G12V/G12V
80
90
100
110
120
130
140
150
160
170
180
190
200
R—R intervals (ms)

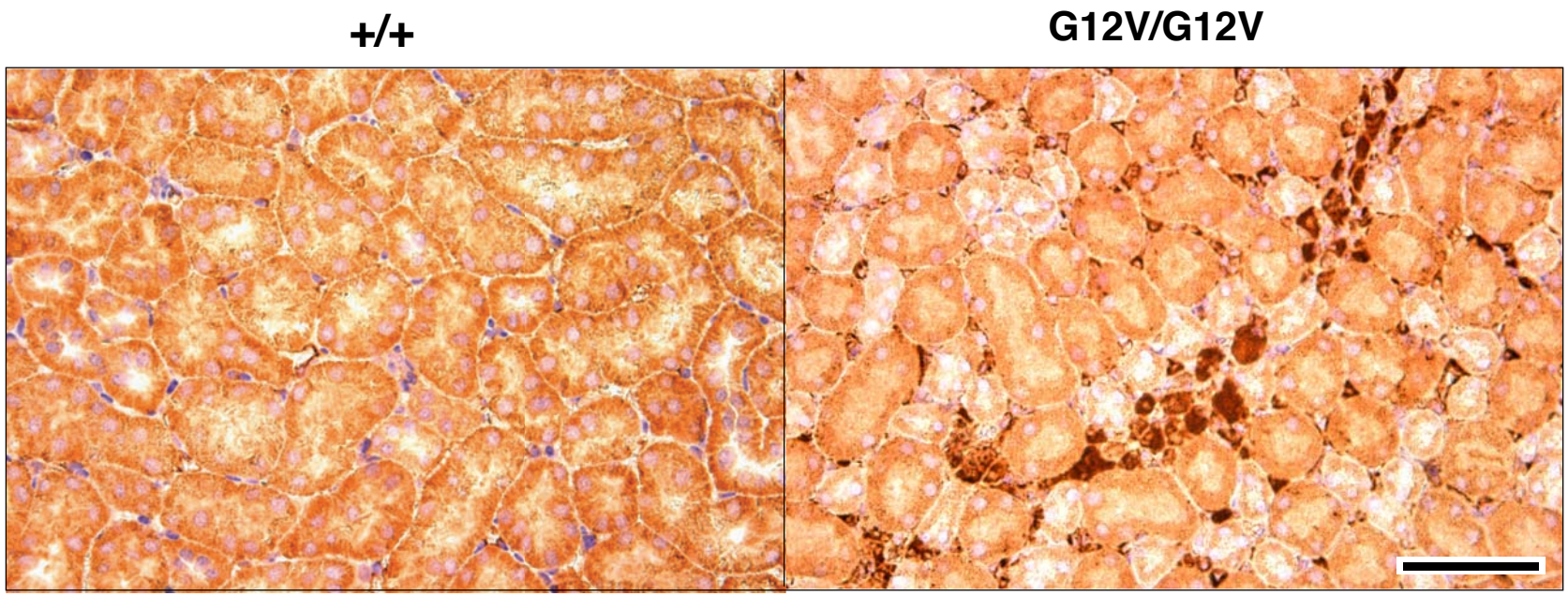
+/+
G12V/G12V

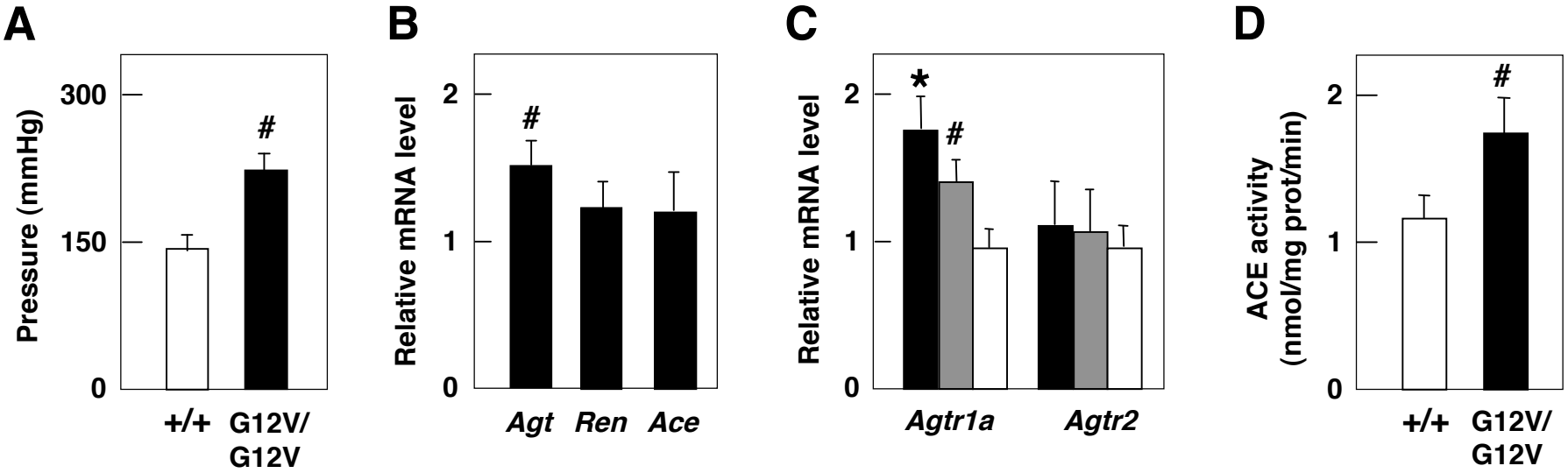
A
Pressure (mmHg)
300
150
0
#
+/+
G12V/
G12V
B
Relative mRNA level
2
1
0
#
Agt
Ren
Ace
C
Relative mRNA level
2
1
0
*
#
Agtr1a
Agtr2
D
ACE activity
(nmol/mg prot/min)
2
1
0
#
+/+
G12V/
G12V